Intermolecular Forces in Argon Van der Waals Complexes. Rotational Spectrum and ab Initio Investigation of Ar-Oxazole†

Elfi Kraka* and Dieter Cremer

Department of Theoretical Chemistry, University of Göteborg, Kemigården 3, 42296 Göteborg, Sweden

Ute Spoerel, Ilona Merke, Wolfgang Stahl, and Helmut Dreizler*

Abteilung Chemische Physik im Institut für Physikalische Chemie der Universität Kiel, D-24098 Kiel, Federal Republic of Germany

Received: February 16, 1995; In Final Form: May 26, 1995[⊗]

The rotational spectrum of the oxazole-argon complex has been experimentally studied in the microwave region between 3 and 21 GHz using a pulsed molecular beam Fourier transform microwave spectrometer. The rotational constants were found to be A = 5012.894 86(14) MHz, B = 1398.428 151(32) MHz, and C = 1388.952 841(31) MHz. The centrifugal distortion constants are D_J' = 5.524 11(28) kHz, D_{JK}' = 37.1990-(30) kHz, D_K' = −35.922(28) kHz, δ_J' = 0.026 26(21) kHz, and R'_6 = −0.000 49(19) kHz. The diagonal elements of the nitrogen quadrupole coupling tensor were determined to be χ_{aa} = 2.3032(6) MHz, χ_{bb} = −4.0526(8) MHz, and χ_{cc} = 1.7494(4) MHz. With the help of supermolecular Møller-Plesset perturbation theory at second (MP2) and fourth order (MP4(SDTQ)) using a (14s10p2d1f)[7s4p2d1f] basis set for argon, a 6-31G(+sd+sp) basis for oxazole, and basis set superposition corrections, stability (MP2, 316; MP4, 304 cm^{-1}), equilibrium geometry, charge distribution, and other properties of the complex were determined. Argon adopts a position above the ring plane (Ar-ring distance: r_0, 3.46; MP2, 3.64; MP4, 3.58 Å) clearly shifted from the centrum of the ring in the direction of the oxygen atom. The complex is predominantly stabilized by dispersion interactions, while the position of the argon atom is determined by exchange repulsion forces that direct Ar toward the O atom. A new way of analyzing van der Waals complexes and predicting structural and other complex properties is presented. Investigation of Ar-oxazole, Ar-benzene, and Ar-CO reveals that there is no charge transfer between the complex partners, contrary to previous claims made in the literature.

1. Introduction

Investigations of van der Waals complexes are one of the challenges of this time, since they lead to a first understanding of the forces that act between molecules in bulk matter.[1] There are four basic components of the interacting energy, namely electrostatic (Coulomb), exchange, induction, and dispersion energy.[2] Each of these components has a different physical origin, magnitude, and directionality. The electrostatic interaction energy E^{es} results from interactions between the permanent electric multipole moments of the complex partners; the induction energy E^{in} results from the permanent electric multipole moments of one monomer with the electric multipole moments induced in the other monomer; the dispersion energy E^{dis} is the result of the mutual polarization of the electron density of the interacting complex partners (interactions of the instantaneous multipoles that are related to dynamic multipole polarizabilities); and the exchange energy E^{ex} is a result of the Pauli principle, which prevents the electrons of one monomer from penetrating into the occupied space of the other monomer. E^{ex} increases with increasing overlap between the two monomer wave functions and is always destabilizing (exchange repulsion or overlap repulsion), contrary to E^{es}, E^{in}, and E^{dis}, which are stabilizing in the case of a van der Waals complex at its equilibrium geometry.[2]

Van der Waals complexes with argon atoms are a particularly rewarding research goal, since a noble gas atom does not possess any permanent electric multipole moments because of its spherical electron density distribution and, accordingly, the electrostatic component is absent in the interaction energy.[3-7] The investigation of the equilibrium geometry of an argon van der Waals complex is rather simple, both from an experimental and a theoretical point of view and provides direct information on the electronic structure of the complex partner. In this way, argon can be considered as a structureless probe of the electronic properties of molecules to which it is bound in a van der Waals complex. The advantage of this approach has been exploited in the investigation of numerous argon van der Waals complexes with di-, tri-, and polyatomic molecules, as is amply documented in recent review articles.[3-7]

Most recently, previous work on Ar van der Waals complexes has been extended to systems involving aromatic rings such as, for example, benzene-argon,[8] fluorobenzene-argon,[9] furan-argon,[10] and pyrrole-argon.[11] It was shown in the case of benzene-argon that the argon atom adopts a position above the center of the aromatic ring. The argon atom is shifted in an off-center position if the benzene ring is substituted, as in fluorobenzene-argon,[9] or replaced by a heteroaromatic system.[10,11] The exact position of the Ar atom indicates features of the π-electron distribution of the aromatic ring and, in addition, provides insight into the differences between in-plane and off-plane approaches (σ- or π-attacks). Investigations of Ar van der Waals complexes involving heteroaromatic systems like furan-argon and pyrrole-argon are particularly interesting, in this connection, and led us to study complexes of argon and heteroaromatic systems containing both nitrogen and oxygen atoms.

In this article, we report on the rotational spectrum, the ^{14}N quadrupole hyperfine structure (hfs), and an ab initio description of oxazole-argon. The measurements of oxazole-argon were

† This paper is dedicated to Professor Dr. John Sheridan, Bangor.

⊗ Abstract published in *Advance ACS Abstracts,* July 1, 1995.

0022-3654/95/2099-12466$09.00/0

TABLE 1: Observed Transitions of Oxazole−Argon

$J''K_a''K_c''-J'K_a'K_c'$	F″−F′	obs (MHz)	obs − calc (kHz)	$J''K_a''K_c''-J'K_a'K_c'$	F″−F′	obs (MHz)	obs − calc (kHz)
110−000	2−1	6 411.1750	0.1	413−404	5−5	3 665.8576	0.0
	1−1	6 411.6994	−0.2		4−4	3 666.7384	0.0
	0−1	6 410.3875	−0.3		3−3	3 665.6314	0.3
111−000	2−1	6 401.9900	0.1	423−414	5−5	10 903.1519	1.3
	1−1	6 400.7740	0.0		4−4	10 903.7889	1.3
	0−1	6 403.8135	−0.1		3−3	10 902.9875	0.7
110−101	2−2	3 623.9315	0.3	422−413	5−5	10 809.2226	1.0
	2−1	3 623.2413	1.2		4−4	10 807.8928	0.4
	1−2	3 624.4552	−0.7		3−3	10 809.5645	1.0
	1−0	3 625.4922	−0.3	505−414	6−5	10 362.1083	0.4
	0−1	3 622.4530	0.1		5−4	10 363.2102	−0.1
220−111	3−2	16 436.6358	−0.4		4−3	10 361.8648	−1.2
	2−1	16 437.1135	−0.6	515−404	6−5	17 481.6628	0.7
	1−0	16 435.2218	−0.7		5−4	17 480.5984	0.1
212−101	3−2	9 179.6307	0.3		4−3	17 481.9205	0.3
	2−1	9 178.3772	0.1	514−505	6−6	3 689.4245	−0.5
	1−0	9 180.9794	0.0		5−5	3 690.3643	0.1
221−110	3−2	16 427.4328	−0.4		4−4	3 689.2342	0.5
	2−2	16 426.6918	−1.0	524−515	6−6	10 925.7072	0.6
	2−1	16 426.1677	−0.3		5−5	10 926.4740	0.3
	1−1	16 427.3192	−0.6		4−4	10 925.5510	0.7
	1−0	16 428.6308	−0.9	523−514	6−6	10 784.8276	−1.0
211−202	3−3	3 633.1228	0.6		5−5	10 783.6043	−0.6
	2−2	3 633.6872	0.2		4−4	10 785.0759	−0.9
	1−1	3 632.8090	0.4	616−505	7−6	20 238.4128	−1.0
220−211	3−3	10 843.7421	−0.3		6−5	20 237.3618	−0.7
	2−2	10 841.7018	0.1		5−4	20 238.6177	−0.8
	1−1	10 844.8758	−0.3	625−616	7−7	10 952.8052	−1.9
221−212	3−3	10 871.7333	−0.6		6−6	10 953.6507	−1.8
	2−2	10 871.5556	−0.1	615−606	6−6	3 718.8419	−1.2
	1−1	10 871.8313	−1.6	716−625	8−7	8 781.9302	−0.5
313−202	4−3	11 952.1877	0.6		7−6	8 783.1425	−0.3
	3−2	11 951.0575	0.3		6−5	8 781.7687	−1.2
	2−1	11 952.7345	0.2	707−616	8−7	15 983.4870	1.3
322−211	4−3	19 204.2142	0.8		7−6	15 984.5363	1.5
	3−2	19 202.9111	0.3		6−5	15 983.3286	0.9
	2−1	19 204.9370	−0.2	817−726	9−8	11 604.6899	0.3
321−212	4−3	19 232.3147	0.3		8−7	11 605.8596	0.4
	3−2	19 232.8827	−0.3		7−6	11 604.5535	−0.5
	2−1	19 231.9989	−0.9	818−725	9−8	11 262.1434	0.2
312−303	4−4	3 647.1027	0.4		8−7	11 261.2159	0.5
	3−3	3 647.8832	0.3		7−6	11 262.2718	−0.5
	2−2	3 646.8293	0.2	808−717	9−8	18 799.4624	0.2
321−312	4−4	10 828.8799	0.8		8−7	18 800.4963	0.5
	3−3	10 827.3437	0.3		7−6	18 799.3275	0.2
	2−2	10 829.4175	0.8	919−826	10−9	14 002.0330	−0.4
322−313	4−4	10 885.1489	0.3		9−8	14 001.0560	0.2
	3−3	10 885.5410	0.5		8−7	14 002.1525	−0.4
	2−2	10 885.0116	0.2	918−827	10−9	14 431.2378	−0.3
414−303	5−4	14 719.5618	0.8		9−8	14 432.3797	0.1
	4−3	14 718.4764	0.4		8−7	14 431.1198	−0.3
	3−2	14 719.9112	0.5				

carried out by means of a molecular beam (MB) Fourier transform microwave (FTMW) spectrometer. The complex was found to be a nearly prolate top with an asymmetry parameter of $\kappa = -0.99$. The rotational constants, centrifugal distortion constants, and diagonal elements of the quadrupole coupling tensor were determined by a least squares fit of all measured hfs components using the program HFS.[12] We found that the observed rotational constants are in agreement with eight different geometries of the complex. The eight geometries form four pairs of enantiomers. Without distinction between the positions below and above the ring plane, the number of geometries reduces to four. Taking also the observed ^{14}N quadrupole coupling constants into account, only two geometries remain, which are consistent with the experimental data. A further distinction was not possible on the basis of the experimental data currently available.

Therefore, an ab initio investigation was carried out using supermolecular Møller−Plesset (MP) perturbation theory[13] at first (MP1 = Hartree−Fock (HF)), second (MP2), third (MP3), and fourth order (MP4) with basis sets especially designed for studies on argon-containing van der Waals complexes. These calculations led to a characterization of the most stable configuration and a description of the forces between the argon atom and the oxazole ring.

In the following, we present results of FTMW measurements (section 2), then a summary of calculational procedures and results (section 3), and finally a discussion of the complex geometry, its properties, and the intermolecular forces stabilizing or destabilizing oxazole−argon (section 4).

2. Experimental Section

All spectra were taken using our MB-FTMW spectrometer[14] in the range from 3 to 21 GHz. For highest resolution and sensitivity, the nozzle was mounted in such a way that the molecular beam propagates along the axis of the cavity from one mirror to the other.[15] Gas mixtures containing 1% oxazole

TABLE 2: Rotational and Centrifugal Distortion (van Eijck) and Quadrupole Coupling Constants of Oxazole−Argon, I^r-Representation[a]

A = 5012.894 86(14) MHz
B = 1398.428 151(32) MHz
C = 1388.952 841(31) MHz
D_J = 5.524 11(28) kHz
D_{JK} = 37.1990(30) kHz
D_K = −35.922(28) kHz
δ_J = 0.02626(21) kHz
R_6 = −0.00049(19) kHz
χ_{aa} = 2.3032(6) MHz
χ_{min} = −5.8020(7) MHz[b]
Calculated
χ_{bb} = −4.0526(8) MHz
χ_{cc} = 1.7494(4) MHz

[a] 103 components fitted; standard deviation = 0.70 kHz. [b] $\chi_{min} = \chi_{bb} - \chi_{cc}$.

(Aldrich, Steinheim) in argon and a stagnation pressure of 50 kPa were used throughout.

2.1. Spectral Analysis. We started our investigation by predicting rotational constants. Therefore we assumed that the geometry of the oxazole molecule, C_3H_3ON, remained unchanged by complexation and that the argon atom was located 3.5 Å above the center of mass of the oxazole. Using the oxazole structure given by Kumar, Sheridan, and Stiefvater,[16] we predicted the rotational constants to be A = 4906 MHz, B = 1396 MHz, and C = 1394 MHz. We further assumed that, due to the rotation of the principal axes, the dipole moment components of oxazole, μ_a = 1.34 D, μ_b = 0.66 D, μ_c = 0 D,[17] should change to μ_a = 0 D, μ_b = 1.34 D, μ_c = 0.66 D for the complex. This should cause a b- and c-type spectrum instead of an a- and b-type spectrum for oxazole. We started our search by scanning the range from 10 418 to 11 020 MHz. Nine lines were found and assumed to be a Q-branch of the complex. They vanished when helium was used as carrier gas. All lines were split into multiplets due to ^{14}N quadrupole coupling. A least squares fit with the program HFS[12] yielded improved rotational constants. With a new prediction, five more lines of a Q-branch in the 3.6 GHz region and the two $J = 1-0$ transitions were found. Again a least squares fit and a new prediction was made so that 18 more P-branch-lines were found. All lines are of b- or c-type; a-type lines were not found in the scanning mode at the prospective frequencies. All measured lines are compiled in Table 1; the rotational and quartic centrifugal distortion constants according to the reduction of van Eijck[18] of oxazole−argon are presented in Table 2. The diagonal elements of the quadrupole coupling tensor were determined by a least squares fit. The results are also presented in Table 2. The corresponding correlation and freedom−cofreedom matrices[19] are given in Table 3.

2.2. Discussion. The spectral analysis led to three rotational constants, five quartic centrifugal distortion constants, and the diagonal elements of the quadrupole coupling tensor. We used the rotational constants to determine the position of the argon atom, assuming that the geometry of the oxazole ring remains unchanged upon complexation. Accordingly, we used for oxazole the geometry given by Kumar, Sheridan, and Stiefvater.[16] Since it was only possible to measure the main isotopomer, we could determine the absolute value but not the sign of the coordinates of the argon position relative to the principal axes of oxazole. Due to the fact that oxazole possesses just a plane of symmetry coinciding with the ring plane, we obtained for the r_0-structure four possible geometries (**1**, **2**, **3**, and **4**) by least squares fit, depending on the initial parameters without distinction of the position above and below the ring plane.

There are four enantiomeric pairs with the argon atom above or below the ring plane. As an example, Figure 1 shows the two enantiomers for geometry **4**. The Ar atom is placed above (or below) the oxazole ring plane at a distance R = 3.458 Å. Geometries **1**−**4** all reproduce the measured rotational constants. The four possible r_0-positions of the argon atom projected onto the oxazole ring plane in the principal inertial system are given in Figure 2 by crosses. We also calculated an "r_S structure" by using the complex isotopomers with argon mass 40, as well as argon mass 0, where the latter case corresponds to oxazole itself. In this case, we cannot assume that the vibrational effects on the moments of inertia partially compensate, since argon with mass 0 causes no vibrational effects. Nevertheless the r_S structures obtained by Kraitchman's substitution formulas[20,21] are in good agreement with the r_0 structures. The r_S type R value is 3.447 Å. It differs from the r_0 value by 0.01 Å. Figure 2 also shows the projected positions of the argon atom (indicated by circles in Figure 2) obtained for the r_S structures.

In order to distinguish between the four possible geometries given in Tables 4 and 5, we tried to get some structural

TABLE 3: Correlation and Freedom−Cofreedom Matrices

Correlation Matrix

A	1.00									
B	−0.04	1.00								
C	0.04	0.30	1.00							
D_J	0.15	0.61	0.77	1.00						
D_{JK}	0.33	0.06	0.36	0.64	1.00					
D_K	0.89	−0.14	−0.14	−0.12	−0.05	1.00				
δ_J	−0.16	0.54	−0.58	−0.20	−0.33	−0.08	1.00			
R_6	−0.23	0.39	−0.53	−0.28	−0.39	−0.13	0.92	1.00		
χ_{aa}	−0.10	−0.02	−0.03	−0.04	−0.06	−0.07	0.02	0.02	1.00	
χ_{min}[a]	0.01	−0.04	0.01	−0.02	−0.03	0.02	−0.05	−0.05	0.03	1.00

Freedom−Cofreedom Matrix

A	0.23									
B	1.00	0.22								
C	0.98	0.87	0.23							
D_J	0.96	0.85	0.77	0.26						
D_{JK}	0.79	0.98	0.93	0.71	0.34					
D_K	0.34	0.99	0.97	0.96	0.81	0.24				
δ_J	0.99	0.67	0.67	0.99	0.97	0.99	0.13			
R_6	0.99	0.84	0.81	0.98	0.96	1.00	0.42	0.26		
χ_{aa}	1.00	1.00	1.00	1.00	1.00	1.00	1.00	1.00	0.99	
χ_{min}[a]	1.00	1.00	1.00	1.00	1.00	1.00	1.00	1.00	1.00	1.00

[a] $\chi_{min} = \chi_{bb} - \chi_{cc}$.

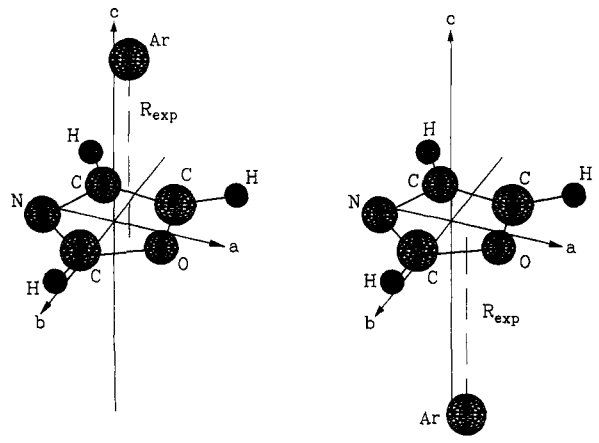

Figure 1. Enantiomer pair of oxazole−argon corresponding to geometry **4**. The coordinate system is the principal axes system of oxazole. The radii of the spheres correspond to the van der Waals radii of the atoms divided by 5. R_{exp} is the distance between Ar and ring plane.

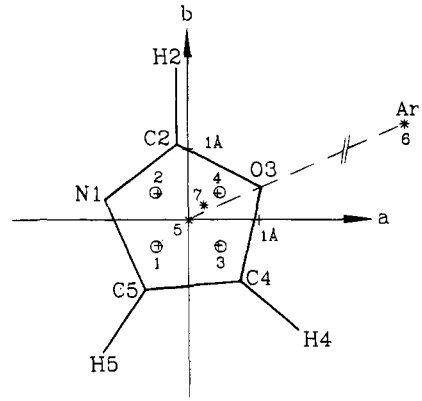

Figure 2. Possible geometries of oxazole−argon. For geometries **1**−**5** and **7**, the projection of the argon atom onto the ring plane of oxazole is indicated by crosses or stars. The coordinate system is the principal axes system of oxazole. Numbering of the ring atoms is shown. r_S geometries **1**−**4** are indicated by circles and the corresponding r_0 geometries by crosses. For geometry **6**, the Ar−O distance has been reduced, indicated by //.

information from the quadrupole coupling tensors of oxazole and oxazole−argon. We assumed that the argon atom does not change the quadrupole coupling tensor of oxazole. So the change of the tensor observed for oxazole−argon, given in Table 2, is merely a consequence of its reference to the different principal axes system of the complex and some vibrational averaging caused by the large amplitude motion of the argon atom. The latter contribution was assumed to be small, and therefore, it was neglected. From our structure determination we know the rotation matrix **D**, which transforms the tensor from the principal axes system of oxazole to the principal axes system of oxazole−argon. The shift of the center of mass is here without influence. We calculated the quadrupole coupling tensor of oxazole−argon, χ_{Ox-Ar}, by transforming the quadrupole coupling tensor of oxazole,[22] χ_{Ox}, by the matrix **D**:

$$\chi_{Ox-Ar} = \mathbf{D}\chi_{Ox}\mathbf{D}^{-1} \quad (1)$$

We tested this method in the case of pyridine and pyridine−argon.[23−25] The quadrupole coupling tensor of pyridine, the result of the rotation, and the experimental quadrupole coupling tensor of pyridine−argon are presented in Table 6. The calculated quadrupole coupling tensors of the four r_S and r_0 geometries are given in Tables 4 and 5. Indeed, two geometries, **2** and **3**, reproduce the quadrupole coupling tensor poorly whereas the other two, **1** and **4**, reproduce it reasonably.

Probably, geometries **1** and **4** do not belong to different stable configurations of the complex; otherwise we should see different

TABLE 4: r_0 Geometries 1−4 of Oxazole−Argon[a]

	a	*b*	*c*	*χ*[b]
			Geometry **1**	
N(1)	−1.1798	0.2733	0.0000	
C(2)	−0.1626	1.0690	0.0000	
O(3)	1.0472	0.4533	0.0000	
C(4)	0.7376	−0.8806	0.0000	$\begin{pmatrix} 2.263 & \pm 0.769^c & \pm 0.249^c \\ & -3.748 & -1.007 \\ & & 1.485 \end{pmatrix}$
C(5)	−0.6096	−1.0006	0.0000	
H(2)	−0.1647	2.1440	0.0000	
H(4)	1.5606	−1.5698	0.0000	
H(5)	−1.2108	−1.8919	0.0000	
Ar	−0.4269	−0.3657	±3.4580[c]	
			Geometry **2**	
	see geometry **1**			$\begin{pmatrix} 2.205 & \pm 0.876^c & \mp 0.533^c \\ & -2.717 & 2.246 \\ & & 0.512 \end{pmatrix}$
Ar	−0.4269	0.3658	±3.4580[c]	
			Geometry **3**	
	see geometry **1**			$\begin{pmatrix} 2.205 & \mp 0.876^c & \pm 0.533^c \\ & -2.717 & 2.245 \\ & & 0.512 \end{pmatrix}$
Ar	0.4269	−0.3658	±3.4580[c]	
			Geometry **4**	
	see geometry **1**			$\begin{pmatrix} 2.263 & \mp 0.769^c & \mp 0.249^c \\ & -3.748 & -1.007 \\ & & 1.485 \end{pmatrix}$
Ar	0.4269	0.3658	±3.4580[c]	

[a] *a*, *b*, and *c* are coordinates in the principal axes system of oxazole. [b] χ is the quadrupole coupling tensor of the complex calculated by rotation of the quadrupole coupling tensor of oxazole. [c] The calculated upper sign belongs to the geometry with the argon atom above the ring plane, and the lower sign to the structure with the argon atom below the ring plane.

TABLE 5: r_S Geometries 1−4 of Oxazole−Argon[a]

	a	*b*	*c*	*χ*
			Geometry **1**	
	see Table 4			$\begin{pmatrix} 2.228 & \pm 0.863^a & \pm 0.338^a \\ & -3.551 & -1.355 \\ & & 1.323 \end{pmatrix}$
Ar	−0.485	−0.383	±3.447[a]	
			Geometry **2**	
	see Table 4			$\begin{pmatrix} 2.159 & \pm 0.944^a & \mp 0.662^a \\ & -2.356 & 2.432 \\ & & 0.197 \end{pmatrix}$
Ar	−0.485	0.383	±3.447[a]	
			Geometry **3**	
	see Table 4			$\begin{pmatrix} 2.159 & \mp 0.944^a & \pm 0.662^a \\ & -2.356 & 2.432 \\ & & 0.197 \end{pmatrix}$
Ar	0.485	−0.383	±3.447[a]	
			Geometry **4**	
	see Table 4			$\begin{pmatrix} 2.228 & \mp 0.863^a & \mp 0.338^a \\ & -3.551 & -1.355 \\ & & 1.323 \end{pmatrix}$
Ar	0.485	0.383	±3.447[a]	

[a] See Table 4 for definitions of *a*, *b*, *c*, χ, and the sign convention.

TABLE 6: Quadrupole Coupling Tensors of Pyridine, χ_{Pyr}, and Pyridine−Argon, χ_{Pyr-Ar}

Measured

$$\chi_{Pyr} = \begin{pmatrix} -4.908 & 0.000 & 0.000 \\ 0.000 & 1.434 & 0.000 \\ 0.000 & 0.000 & 3.474 \end{pmatrix} \quad \chi_{Pyr-AR} = \begin{pmatrix} 3.365 & & \\ & -4.805 & \\ & & 1.441 \end{pmatrix}$$

Calculated Pyridine−Argon[a]

$$\chi_{calc} = \begin{pmatrix} 3.417 & \mp 0.689^b & 0.000^c \\ \mp 0.689^b & -4.851 & 0.000^c \\ 0.000^c & 0.000^c & 1.434 \end{pmatrix}$$

[a] Calculated by transformation of χ_{Pyr} into the principal axes system of pyridine−argon. [b] See Table 4. [c] The elements χ_{ac} and χ_{bc} are zero due to symmetry.

spectra caused by different centrifugal distortion constants due to the different positions of the argon atom. We did not observe any effect like this. Also no line broadening or splitting was observed, which should have been detected if the two positions were connected by a double minimum potential. Nevertheless, we were unable to distinguish between geometries **1** and **4**. Investigations of furan−argon and pyrrole−argon[10,11] showed that the Ar atom is shifted toward the electronegative part of the ring. Therefore it seems reasonable to favor geometry **4**. In this geometry, the Ar atom is closer to oxygen than it is to nitrogen in geometry **1**.

3. Ab Initio Calculations

Theoretical calculations of van der Waals complexes based on supermolecular perturbation theory have to fulfill four basic requirements: (1) The basis set used has to be flexible enough to reproduce the different contributions to the interaction energy. (2) All calculations have to be corrected for basis set superposition errors (BSSEs); that is, calculations have to be basis set consistent.[26] (3) The order of the perturbation theory has to be high enough to ensure convergence of the calculated interaction energy. (4) The method used has to be size extensive, which is guaranteed for many body perturbation theory and coupled cluster theory but may become a problem if one has to go beyond these levels of theory.

Although it is not difficult to provide a sufficient description of exchange effects because these are typical short range effects, the correct description of electrostatic, inductive, and dispersion effects cannot be achieved with standard basis sets.[3] In particular, the description of electrostatic and dispersion effects turns out to be rather difficult. Since the former is of no relevance for Ar−oxazole, the basis set problem may be considered somewhat easier to solve. Nevertheless, the basis set has to be chosen to reproduce multipole moments and polarizabilities of the monomers and to recover large portions of the dispersion energy, which normally requires a basis set of at least TZ+2P quality.[3] Such a basis is already too large to be used for extended scanning of the potential energy surface (PES) of Ar−oxazole at the MP2 level of theory. Therefore, we have chosen a somewhat different approach.

First, we have tested various basis sets with regard to their ability to reproduce the experimental value of the static dipole polarizability α of Ar[27] both at the HF and MP2 levels of theory. The polarizability α is a molecular property that is related to the molecular volume, which in turn can be described by the 0.001 au contour level of the molecular electron density distribution.[28] This means that contrary to energy or geometry, which predominantly depends on the electron density distribution in the valence region, the polarizability is sensitive to diffuse density distributions in the tail region of the wave function. This is best reflected by the fact that energy-optimized basis sets such as 6-31G(d) or 6-311G(d),[29] lead to rather poor values of α(Ar) more than 50% lower than the experimental value (11.09 bohr,[3,27] Table 7) irrespective of the method chosen. More reliable values are already obtained at the HF level by employing large basis sets with diffuse basis functions as well as multiple sets of d- and f-type polarization functions. For example, with the generally contracted (17s12p5d4f)[7s7p5d4f] atomic natural orbital (ANO) basis set of Roos and co-workers,[30] the polarizability of Ar can be reproduced with an error of about 4% (Table 7). Very reliable values for α are calculated using an extremely large basis set with 118 basis functions, such as the (15s12p5d4f3g)[11s9p5d4f3g] basis of Thakkar and co-workers,[31] which has been derived from a (14s11p)[10s8p] Huzinaga basis by adding a set of diffuse sp functions and various sets of d-, f-, and g-type polarization functions. Finite field MP4 (FF-MP4),[32] coupled cluster with SD excitations and a perturbational treatment of the T excitations, CCSD(T),[33] or constrained dipole oscillator strength distribution (DODS)[34] calculations lead to α = 11.1 or 11.2 bohr,[3] in perfect agreement with the experimental value.

TABLE 7: Static Dipole Polarizabilities α (bohr^3) of Ar Calculated with Different Basis Sets at Different Levels of Theory[a]

method	basis set	#BF	α	ref
HF	6-31G(d)	13	4.01	this work
HF	6-311G(d)	26	3.46	this work
HF	(14s10p2d1f)[7s4p2d1f]	36	9.57	this work
HF	(17s12p5d4f)[6s5p2d1f]	38	9.87	this work
HF	(17s12p5d4f)[6s6p3d2f]	53	10.69	this work
HF	(17s12p5d4f)[6s6p4d3f]	65	10.72	this work
HF	(17s12p5d4f)[7s7p5d4f]	98	10.72	this work
MP2	6-31G(d)	13	3.99	this work
MP2	6-311G(d)	26	3.41	this work
MP2	(14s10p2d1f)[7s4p2d1f]	36	9.98	this work
MP4(SDTQ)	6-31G(d)	13	4.01	this work
QCISD	6-31G(d)	13	4.02	this work
FF-MP4	(15s12p5d4f3g)[11s9p5d4f3g]	118	11.23	33
CCSD(T)	(15s12p5d4f3g)[11s9p5d4f3g]	118	11.21	33
DOSD	(15s12p5d4f3g)[11s9p5d4f3g]	118	11.08	33
exp			11.09	27

[a] Basis sets 6-31G(d) and 6-311G(d) from ref 29; basis set [7s4p2d1f] from ref 35; basis sets [6s5p2d1f], [6s6p3d2f], [6s6p4d3f], and [7s7p5d4f] from ref 30; basis set [11s9p5d4f3g] from ref 31. #BF denotes the number of basis functions.

Neither large ANO basis sets nor the standard DZ+P basis sets are suitable for large scale investigations of Ar van der Waals complexes, since they are either too large or too inaccurate. Better suited are basis sets that have been particularly chosen to calculate polarizabilities and dispersion energies, such as the (14s10p2d1f)[7s4p2d1f] basis set of Chalasinski, Funk, and Simons[35] derived from a (14s10p) energy-optimized Rosendaal basis.[36] In order to allow for deformation of the Ar orbitals in the Ar_2 van der Waals complex, the two most diffuse sp functions of the (14s10p) basis remained uncontracted while the exponents of added d- and f-type polarization functions were optimized to accurately describe the dispersion energy of Ar_2. Although the resulting DZ+(2d1f) basis set is of moderate size (36 basis functions for Ar), it reproduces the Ar polarizability at the MP2 level with an accuracy of 96% (Table 7). Therefore, we have chosen the (14s10p2d1f)[7s4p2d1f] basis of Chalasinski, Funk, and Simons as the appropriate Ar basis for our Ab initio investigation of the Ar−oxazole complex.

As for the oxazole ring, we have tested various basis sets, again with regard to their ability to reproduce experimental polarizabilities and dipole and quadrupole moments. In their investigation of benzene−Ar and fluorobenzene−Ar, Hobza and co-workers[37] have suggested a 6-31+G(d) basis based on Pople's 6-31G basis.[29] The exponent of the diffuse sp functions was set equal to $^1/_3$ of the value of the outermost sp function of the original 6-31G basis. In addition, the d exponent was chosen to be 0.25, which is about one third of its original value of 0.8 in Pople's 6-31G(d) basis. Although of modest size, this 6-31+G(d) basis leads to a rather accurate polarizability and quadrupole moment for benzene.[37] However, a disadvantage of the Hobza basis is that the composition of the basis has been done in an ad hoc manner, which does not give a clear directive on how to construct the basis set for heteroatoms such as O, N, S, etc.

A systematic approach to developing moderately sized basis sets for calculations of polarizabilities has been suggested by Spackman.[38] He advocates a 6-31G(+sd,+sp) basis obtained

TABLE 8: Experimental and Theoretical Geometries of Oxazole[a]

	exp[b]	HF/6-31G-(+sd,+sp)	MP2/6-31G-(+sd,+sp)	MP2/6-31G(d)
R(N−C2)	1.291	1.282	1.329	1.304
R(C2−O)	1.357	1.361	1.420	1.361
R(O−C4)	1.370	1.386	1.426	1.371
R(C4−C5)	1.352	1.339	1.380	1.361
R(C5−N)	1.396	1.410	1.434	1.390
R(C2−H2)	1.075	1.067	1.088	1.080
R(C4−H4)	1.073	1.065	1.087	1.078
R(C5−H5)	1.075	1.067	1.089	1.080
α(N−C2−O)	114.9	113.2	113.9	114.9
α(C2−O−C4)	103.9	105.2	103.7	103.8
α(O−C4−C5)	108.1	107.2	107.9	107.9
α(C4−C5−N)	109.0	108.9	109.8	109.4
α(C5−N−C2)	103.9	105.3	104.6	103.8
α(C4−C5−H5)	129.0	129.4	128.8	128.9
α(C5−C4−H4)	135.0	135.4	136.1	135.6
α(N−C2−H2)	127.9	128.8	129.6	128.6

[a] Bond lengths R in Å; bond angles α in deg. For numbering of atoms see Figure 2. [b] r_S geometry from ref 40.

from Pople's 6-31G basis by adding diffuse polarization functions as well as a diffuse s function. The exponents of the d-type polarization functions for first- and second-row atoms, as well as of the p-type polarization functions for hydrogen, were optimized with respect to maximizing the mean polarizability of first- and second-row AH_n hydrides.[38] The exponent of the diffuse s function was set equal to $^1/_4$ of the value of the outermost sp functions of the original 6-31G basis, while the exponent of the diffuse s function for hydrogen was set equal to 0.040. With this basis set, HF polarizabilities with an error of less than 15% and MP2 polarizabilities accurate up to 5% are obtained. Therefore, we have chosen the 6-31G(+sd,+sp) basis of Spackman for our investigation but have checked its results in selected cases by also using the Hobza 6-31+G(d) basis extended to heteroatoms.

According to the counterpoise procedure (CP) of Boys and Bernardi,[39] both the complex and monomers should be calculated with the dimer-centered basis set (DCBS) to avoid basis set superposition errors (BSSEs).[26] In particular for moderately sized basis sets, CP corrections are essential for supermolecular perturbation theory. In the case of the Ar−oxazole complex the BSSE leads to changes of the interaction energy by 100−150% and changes in the geometry by 50%. There are been discussions that the CP method overestimates BSSEs and, accordingly, leads to reduced complex interaction energies. However, recent investigations suggest that the CP method, even if it marginally overestimates BSSEs, is definitely the most reliable correction procedure.[26] Therefore, all calculations including property calculations and geometry optimizations of the Ar−oxazole complex were carried out with the CP method of Boys and Bernardi using the DCBS.

Only limited geometry optimizations have been carried out, since it is reasonable that the oxazole geometry is retained in the complex. Geometry optimizations of oxazole at the HF and MP2 level of theory lead to geometrical parameters that differ considerably (Table 8), where only the HF geometry is close to the r_S geometry determined by MW spectrometry.[16,40] This seems surprising because MP2 geometries are normally more accurate than HF geometries.[41] However, we have to stress that the 6-31G(+sd,+sp) basis set is no longer energy optimized, contains a relatively large number of diffuse functions, and therefore, leads to an expansion of the electron density distribution, which is accompanied by the nuclei to some extent thus yielding rather large bond lengths. This is confirmed by a determination of the equilibrium geometry at the MP2/6-31G-(d) level of theory (see Table 8). MP2/6-31G(d) bond lengths and angles agree better with experimental r_S values than either HF or MP2 values obtained with the 6-31G(+sd+sp) basis. Because of this, we have used the experimental r_S geometry in all calculations.

The position of the Ar atom was determined by establishing a grid of points above the plane of the oxazole ring. These points include the four positions of Ar belonging to geometries **1**, **2**, **3**, and **4**, a position of Ar above the center of mass of the five-membered ring (geometry **5**), a position of the Ar atom in the ring plane opposite the O atom (geometry **6**), the equilibrium position of Ar (geometry **7**), as well as intermediate points (see Figure 2). For each position, the distance R from the ring plane was optimized considering BSSEs by the CP procedure. These calculations indicated already that there is only one minimum position above the ring plane, the exact position of which was determined by fitting calculated energy points with optimized R values to a two-dimensional function and calculating the minimum of this function. The final energy calculation was performed using the optimized position of the Ar atom.

Qualitative descriptions of van der Waals complexes that are stabilized by multipole interactions can already be obtained at the HF level of theory.[3] However, if dispersion forces dominate the complex stability, it is necessary to use a correlation-corrected method. We applied MP2, MP3, and MP4 perturbation theory,[13] where in the latter case single (S), double (D), triple (T), and quadrupole (Q) excitations, {MP4(SDTQ)}, were included. Interaction energies calculated at the HF = MP1, MP2, MP3, MP4(SDQ), and MP4(SDTQ) levels were compared to check their reliability.

All calculations have been carried out with the ACESII[42] and the COLOGNE94[43] ab initio packages.

4. Results and Discussion

In Table 9, optimized R values for geometries **1**−**7** (Figure 2) are given together with absolute and relative energies obtained at the various levels of theory.

At the HF level, a minimum for the Ar−oxazole complex with the Ar atom placed either above or in the plane of the oxazole ring could not be found. Obviously, exchange repulsion effects are larger than stabilizing inductive effects (dispersion effects are not covered at the HF level). However, at the MP2 level, the Ar atom is bound to the ring by about 240−320 cm^{-1} (700−900 cal/mol) regardless of whether geometry **1**, **2**, **3**, or **4** is adopted. The optimized R value varies from 3.51 Å (position **3**) to 3.61 Å (position **2**); that is, in all cases the calculated distance between Ar and the ring plane is larger than the experimental r_0 value of 3.458 Å. In the case of geometry **4**, R(MP2) is exactly 0.1 Å larger, although, at the MP3 and MP4(SDQ) levels, R of geometry **4** increases to 3.64 Å. The inclusion of T excitations at the MP4 level reduces R to 3.580 Å, which is close to the MP2 value.

At all levels of theory considered, geometry **4** corresponds to the most stable complex configuration. Its relative energy is 316 cm^{-1} (904 cal/mol) at the MP2 level and 292 cm^{-1} (835 cal/mol) at the MP4 level, while intermediate levels lead to smaller binding energies in line with an increase of R at these levels of theory. The similarity of MP2 and MP4 complexation energies and optimized R values suggests that supermolecular perturbation theory at the MP2 level is sufficient to mimic the more accurate MP4 results.

Differences in the energies between geometries **1**−**4** range from 22 to 48 cm^{-1} (63 to 138 cal/mol). If one places the Ar atom exactly above the ring center (geometry **5**), which is close to the position in **4**, the difference in energies reduces to just 2

TABLE 9: Stabilization Energies ΔE of Oxazole−Argon for Geometries 1−7 at Experimental Distances R_{exp} and Optimized Distances R_{opt} Evaluated at Different Levels of Møller−Plesset Perturbation Theory Using the 6-31G(+sd,+sp) Basis[a]

			R_{exp} = 3.485						
method	geometry	Ar closest to	ΔE	$\Delta\Delta E$	R_{opt}	a	b	ΔE	$\Delta\Delta E$
MP2	1	C5	−250	70	3.528	−0.453	0.333	−268	48
	2	N	−287	33	3.615	0.260	0.499	−294	22
	3	C4	−252	68	3.514	−0.260	−0.499	−277	40
	4	O	−320	0	3.558	0.453	−0.333	−316	0
	5	center	−309	11	3.595	0.	0.	−314	2
	6	in-plane, at O			3.646			−121	195
	7, min	O			3.538	0.226	−0.167	−322	−6
MP3	4	O	−178		3.637			−235	
MP4(SDQ)	4	O	−208		3.636			−237	
MP4(SDTQ)	4	O	−292		3.580			−304	

[a] Relative energies ΔE in cm^{-1}; R and coordinates a and b in Å (see Figure 2). The HF, MP2, MP3, MP4(SDQ), and MP4(SDTQ) energies of geometry **4** are as follows: from calculations with R_{exp}, −771.311 09, −772.028 51, −772.043 36, −772.059 32, and −772.089 58 hartrees; and calculation from calculations with R_{opt}, −771.311 29, −772.028 96, −772.042 11, −772.058 09, and −772.267 89 hartrees.

cm^{-1} (7 cal/mol), indicating the flatness of the PES with regard to horizontal displacements of Ar. Optimization of the position of the Ar atom leads to an energy minimum of −322 cm^{-1} (−922 cal/mol) located in the vicinity of geometry **4** about halfway in the direction of a point that lies exactly above the center of mass of the oxazole ring. The R value of the minimum-energy geometry (**7** in Table 9) is 3.54 Å, which is 0.02 Å shorter than for geometry **4**.

If Ar is placed in the plane of the ring opposite to the O atom (geometry **6**), a relatively large distance of 3.64 Å is calculated. The complex stability decreases to 121 cm^{-1} (345 cal/mol), indicating that positions above and below the ring plane are energetically favored compared to positions in the ring plane (see below). We also tested energy differences by using the 6-31+G(d) basis of Hobza and co-workers[37] for the ring and obtained similar results. In conclusion, the ab initio geometry **7** confirms the selection of the experimentally determined geometry **4** as the most likely configuration of the Ar−oxazole complex.

Scanning of the PES in the region of geometries **1**−**5** reveals that there is only one minimum at position **7**. Complex form **6** with the Ar atom in the ring plane is more than 200 cm^{-1} (577 cal/mol) higher in energy than the equilibrium form (geometry **7**), and therefore, form **6** is unlikely to be seen in molecular beam experiments. Since geometries **1**, **2**, and **3** are not connected with stationary points on the PES, theory and experiment are in agreement insofar as only one complex form has been detected spectroscopically.

From comparison of interaction energies obtained at various orders of supermolecular perturbation theory with the corresponding interaction energies obtained by symmetry-adapted (intermolecular) perturbation theory,[6] one knows that, for a complex such as Ar−oxazole, the supermolecular HF interaction energy comprises basically the Heitler−London exchange repulsion energy and the induction energy apart from various exchange-deformation energies.[3,6] At the MP2 level, correlation corrections are added to exchange repulsion and inductive effects, but in addition the dispersion energy is covered by the calculated interaction energy. At MP3 and MP4 levels higher order corrections to the three basic interaction components as well as couplings between them are included.[3,6] Hence, the mere fact that oxazole−Ar is not stable at the HF level but substantially stabilized at the MP2 level indicates that the complex is dispersion bound, which is in line with observations made for other Ar van der Waals complexes.[3] Of course, corrections to inductive effects could also lead to stabilization, but we doubt this for the following reason. Since oxazole possesses sizable dipole and quadrupole moments (Table 10),

TABLE 10: Polarizability α (bohr³), Dipole Moment μ (D), and Quadrupole Moment Q (10^{-26} esu cm²) of Oxazole in Its Principal Inertial Axis System[a]

	experimental values[a]	experimental geometry		optimized geometry	
		HF	MP2	HF	MP2
α		41.27	42.75	40.92	45.00
μ_a	−1.365(20)	−1.34	−1.49	−1.44	−1.44
μ_b	−0.630(20)	−0.64	−0.78	0.49	−0.65
μ_{tot}	1.503	1.49	1.68	1.52	1.58
Q_{aa}	−4.9(29)	−6.28	−5.97	3.50	−5.52
Q_{bb}	9.5(31)	9.53	8.57	−0.04	9.56
Q_{cc}	−4.6(49)	−3.23	−2.60	−3.47	−4.04
Q_{ab}		0.32	0.22	8.23	4.09

[a] Values are given for experimental and HF- and MP2-optimized geometries using the 6-31G(+sd,+sp) basis set. [b] Dipole moment from ref 17; quadrupole moment from ref 40.

the induction energy of the oxazole−Ar complex should be dominated by the three energy terms in eqs 2−4.[2]

$$E^{ind}(\mu) = -\sum_q \{\mu_q^2(\text{oxazole})\alpha(\text{Ar})(3\cos^2\theta + 1)/(2r^6)\} \quad (2)$$

$$E^{ind}(\mu Q) = -\sum_q \{3\mu_q(\text{oxazole})Q_{qq}(\text{oxazole})\alpha(\text{Ar})\cos^3\theta/r^7\} \quad (3)$$

$$E^{ind}(Q) = -\sum_q \{9Q_{qq}^2(\text{oxazole})\alpha(\text{Ar})[1 - 2\cos^2\theta + 5\cos^4\theta]/(8r^8)\} \quad (4)$$

where μ_q and Q_{qq} are the components of the dipole and quadrupole moments, r is the distance between Ar and the center of mass of the oxazole ring, and θ is the angle between the position vector of the Ar atom given in the coordinate system of Figure 2 and the respective principal axis $q = a$, b, or c of oxazole. For reasons of simplicity, the assumption has been made that the oxazole ring can be modeled by a cylindrical charge distribution with $Q_{pq} = 0$ for $q \neq p$.[2] Using the experimentally determined dipole and quadrupole moments of oxazole (Table 10), the experimental polarizability of Ar, α(Ar), the distance R_{exp} for r, $\theta = 90°$ for $q = a$, b, and $\theta = 0°$ for $q = c$ (position **5**), induction energies of −6, 0, and −92 cm^{-1} (−16, 0, and −264 cal/mol) are obtained for the three energy terms of eqs 2, 3, and 4. Obviously, the total stabilization of −98 cm^{-1} (−279 cal/mol) is annihilated by overlap repulsion effects at the HF level.

When going from the HF level to the MP2 level, the oxazole dipole moment is slightly increased while components of the

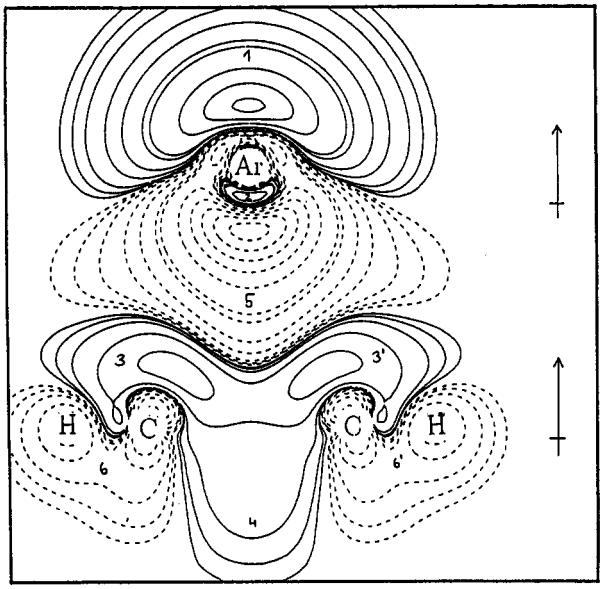

Figure 3. Contour line diagram of the MP2 difference electron density distribution of benzene−argon, $\Delta\varrho(\mathbf{r}) = [\varrho(\text{benzene−argon}) - \varrho(\text{benzene})^{DCBS} - \varrho(\text{argon})^{DCBS}]$, using the 6-31G(+sd,+sp) basis for benzene and the [7s4p2d1f] basis for argon. The reference plane is the plane perpendicular to the benzene ring that contains Ar and two CH bonds. Contour lines range from 2×10^{-6} to 2×10^{-1} [e/bohr^3]. Solid lines correspond to an increase of electron density upon complex formation, and dashed lines to a decrease. Regions of increase and decrease of electron density are marked by small numbers. The direction of the induced monomer dipole moments is schematically indicated by arrows.

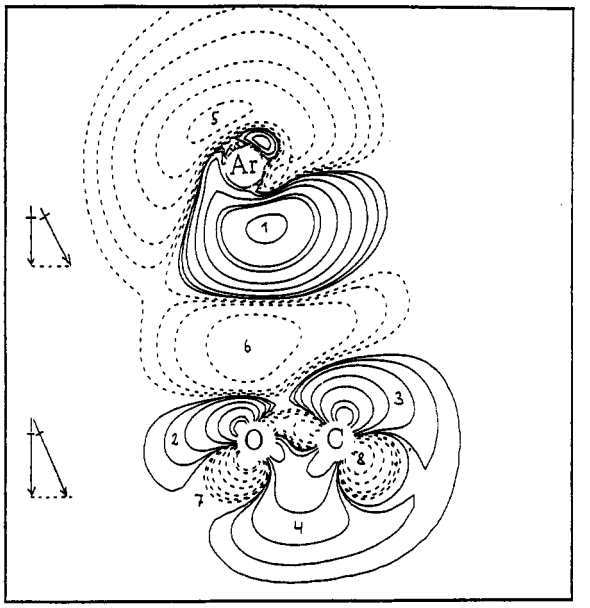

Figure 4. Contour line diagram of the MP2 difference electron density distribution of Ar−CO, $\Delta\varrho(\mathbf{r}) = [\varrho(\text{Ar−CO}] - \varrho(\text{Ar})^{DCBS} - \varrho(\text{CO})^{DCBS}]$, using the 6-31G(+sd,+sp) basis for CO and the [7s4p2d1f] basis for argon. The reference plane is the plane of the three nuclei. Contour lines range from 2×10^{-6} to 2×10^{-1} [e/bohr^3]. Solid lines correspond to an increase of electron density upon complex formation, and dashed lines to a decrease. Regions of increase and decrease of electron density are marked by small numbers. The direction of the induced monomer dipole moments as their components is schematically indicated by arrows.

quadrupole moment are decreased (Table 10). Induction effects in total are decreased by 10−20%. This value can be used as a guideline for corrections to the total multipole induction obtained at the MP2 level, which accordingly cannot be very large. Destabilizing exchange repulsions should increase at the MP level, since the occupied space of a molecule increases at the correlation level, probably annihilating additional stabilization caused by charge polarization.

It remains to be clarified which effect leads to a preference of geometries **4** and **7**. To answer this question, we use the electron density analysis as an investigative tool. In Figure 3, a contour line diagram of the MP2 difference electron density distribution

$$\Delta\varrho(\mathbf{r}) = [\varrho(\mathbf{r})\text{complex}] - [[\varrho(\mathbf{r})\text{monomer}]^{DCBS} + [\varrho(\mathbf{r})\text{Ar}]^{DCBS}] \quad (5)$$

of the benzene−Ar complex is given with regard to a plane containing the Ar atom, the center of the benzene ring, and two CH bonds. The diagram reveals a regular pattern of regions with increase (solid contour lines) and decrease (dashed contour lines) of electron density because of complex formation. Electron density is pushed out of the intermolecular region (region 5 in Figure 3) toward the back of the Ar atom (region 1) and through the center of the benzene ring (region 4). If a nucleus stops this movement of negative charge, a buildup of negative charge can be found in front of the nucleus. Hence, large regions of charge buildup can be found in front of the C atoms (regions 3 and 3′), and a smaller region can be found in front of the Ar atom (region 2).

The difference density distribution is a result of exchange repulsion and mutual charge polarization. Destabilizing exchange repulsion is smallest above the ring center, while dispersion effects should be larger above the C atoms. According to both experimental and theoretical investigations of Hobza and co-workers,[37a] Ar prefers the position above the ring center, which can be easily explained on the basis of the difference electron density distribution of Figure 3. Polarization of the electron charge clouds of benzene and Ar (regions 1−6, Figure 3) leads to monomer dipole moments in the complex that possess directions directly reflected by the difference density. The positive end of the Ar dipole is at the benzene side while the negative end of the benzene dipole is at the Ar side; that is, the two dipoles attract each other (Figure 3) and form in sum a small dipole moment directed from benzene to Ar. This dipole moment is somewhat diminished by the buildup of negative charge in regions 2 and 4.

The MP2 dipole moment of the benzene−Ar complex (0.092 D) is directed exactly as predicted according to the difference electron density distribution of Figure 3. However, it contradicts the calculational results of Hobza, Selzle, and Schlag, who have found a charge transfer of 0.018 electron from the benzene ring to the Ar atom, suggesting the formation of a donor−acceptor or charge transfer complex. We have checked this hypothesis by analyzing Mulliken population values at the MP2 level and find a similar charge transfer, which vanishes when the population values are properly corrected with the counterpoise procedure. *Ar remains electroneutral.* The description of benzene−Ar as a charge transfer complex is not correct. The complex is stabilized by dispersion and inductive effects. Exchange repulsion is destabilizing, but it directs Ar above the center of the ring to a position where exchange repulsion should be weakest, although dispersion and inductive interactions should be encountered with all six C atoms.

The discussion of the Ar−benzene complex suggests that the most favorable position of the Ar atom should be above the oxazole ring somewhere close to a position above the center of the ring. However, it is not clear why a position closer to the O atom is preferred. To clarify this we discuss the MP2 difference electron density distribution of the Ar−CO van der Waals complex shown in Figure 4.

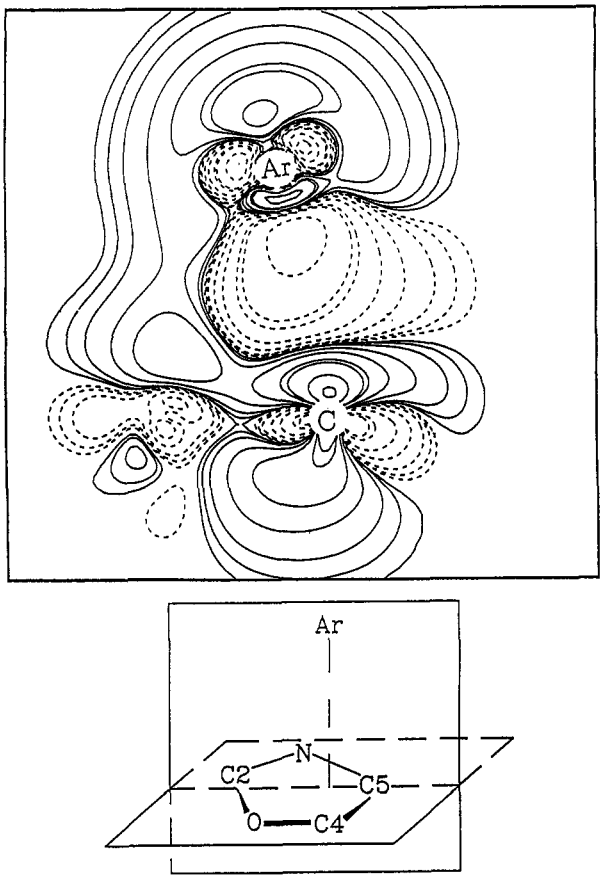

Figure 5. Contour line diagram of the MP2 difference electron density distribution of oxazole−argon, $\Delta\varrho(\mathbf{r}) = [\varrho(\text{oxazole−argon}) - \varrho(\text{oxazole})^{DCBS} - \varrho(\text{argon})^{DCBS}]$, using the 6-31G(+sd,+sp) basis for oxazole and the [7s4p2d1f] basis for argon. The reference plane contains Ar and C5, as is schematically indicated in the figure. Contour lines range from 2×10^{-6} to 2×10^{-1} [e/bohr^3]. Solid lines correspond to an increase of electron density upon complex formation, and dashed lines to a decrease.

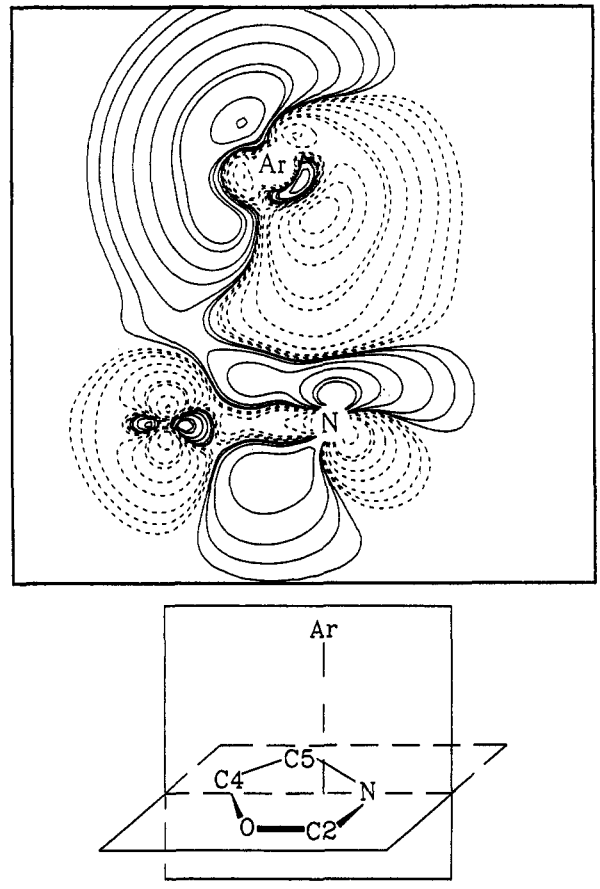

Figure 6. Contour line diagram of the MP2 difference electron density distribution of oxazole−argon, $\Delta\varrho(\mathbf{r}) = [\varrho(\text{oxazole−argon}) - \varrho(\text{oxazole})^{DCBS} - \varrho(\text{argon})^{DCBS}]$, using the 6-31G(+sd,+sp) basis for oxazole and the [7s4f2d1f] basis for argon. The reference plane contains Ar and N, as is schematically indicated in the figure. Contour lines range from 2×10^{-6} to 2×10^{-1} [e/bohr^3]. Solid lines correspond to an increase of electron density upon complex formation, and dashed lines to a decrease.

Ar−CO possesses a distorted T structure (Ar sitting on the CO bond) with the Ar atom being closer to the O rather than the C atom.[3,44] The difference electron density distribution again reveals a pattern of regions (1−8, Figure 4) with buildup or depletion of negative charge. However, the pattern is quite different from that of the benzene−Ar complex. Negative charge seems to be pulled from the backside of the Ar atom (region 5) to the frontside (region 1). This effect is more pronounced opposite to the O atom than opposite to the C atom. At the CO molecule, there is charge built up in a smaller region (region 2) in front of the O atom and in a larger region (region 3) in front of the C atom. In addition, it seems as if bonding and lone pair density have been pushed toward region 4 on the backside of the CO molecule.

The various components of the interaction energy that determine the complex stability in the case of the Ar−CO complex have been studied in detail, and therefore, one knows that dispersion effects are largest at the C atom because of the larger polarizability of its negative charge cloud. However, exchange repulsion is smaller and less destabilizing at the O than at the C atom. If the Ar atom approaches the CO molecule in a direction perpendicular to the CO bond, its electron cloud "sees" at the C site a relatively extended charge cloud while at the O atom negative charge is pressed more against the O atom. One can speak of an O-centered hole in the charge cloud of the CO molecule, toward which some of the negative charge of Ar is drawn. As a consequence, the dipole components perpendicular to the CO bond axis at Ar and at CO have the opposite direction compared to the situation for benzene−Ar (see Figures 3 and 4), and the component of the total dipole moment of the complex in this direction has its positive end at Ar and its negative end at CO. We obtain a MP2 dipole moment of 0.357 D with components of −0.356 and 0.023 D parallel and perpendicular to the CO axis. After CP corrections, Mulliken population values indicate no charge transfer.

Clearly, the position of the Ar atom is determined by exchange repulsion effects that are smaller and less destabilizing opposite to the O atom. This is reflected exactly by the difference electron density distribution shown in Figure 4, which suggests that the Ar−oxazole complex should be investigated in a similar way. In Figures 5−8, contour line diagrams of the MP2 difference electron density distribution of the Ar−oxazole complex are shown with regard to reference planes that are perpendicular to the plane of the oxazole ring and contain both the Ar nucleus and the nucleus of the atom next to the Ar atom; that is, reference planes for geometries **1**−**4** contain besides the Ar nucleus also that for C5, N, C4, and O. In this way the difference density plots in Figures 5−8 provide information about the major interaction effects.

Inspection of the contour line diagrams in Figures 5−8 immediately reveals that there is a hole in the electron distribution above the O atom similar to that observed in the case of the Ar−CO complex. In the oxazole−Ar complex the negative charge of Ar is polarized in this direction, indicating that exchange repulsion effects are smaller in the region between Ar and oxygen and that a buildup of negative charge in the

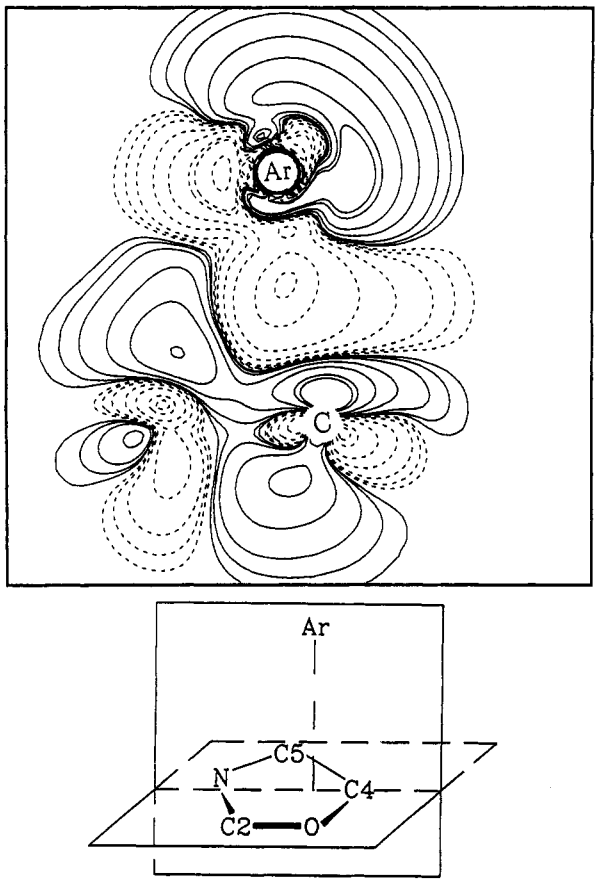

Figure 7. Contour line diagram of the MP2 difference electron density distribution of oxazole−argon, $\Delta\varrho(\mathbf{r}) = [\varrho(\text{oxazole−argon}) - \varrho(\text{oxazole})^{DCBS} - \varrho(\text{argon})^{DCBS}]$, using the 6-31G(+sd,+sp) basis for oxazole and the [7s4f2d1f] basis for argon. The reference plane contains Ar and C4, as is schematically indicated in the figure. Contour lines range from 2×10^{-6} to 2×10^{-1} [e/bohr^3]. Solid lines correspond to an increase of electron density upon complex formation, and dashed lines to a decrease.

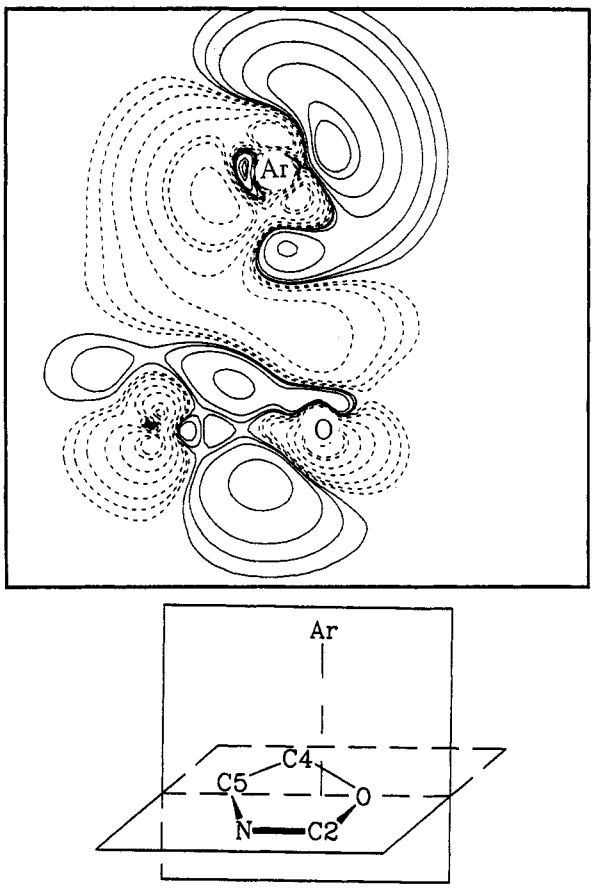

Figure 8. Contour line diagram of the MP2 difference electron density distribution of oxazole−argon, $\Delta\varrho(\mathbf{r}) = [\varrho(\text{oxazole−argon}) - \varrho(\text{oxazole})^{DCBS} - \varrho(\text{argon})^{DCBS}]$, using the 6-31G(+sd,+sp) basis for oxazole and the [7s4p2d1f] basis for argon. The reference plane contains Ar and O, as is schematically indicated in the figure. Contour lines range from 2×10^{-6} to 2×10^{-1} [e/bohr^3]. Solid lines correspond to an increase of electron density upon complex formation, and dashed lines to a decrease.

region between the Ar and O atoms is possible (Figure 8). In none of the other three cases can a comparable buildup be found. Instead, in geometries **1** and **2** (Figures 5 and 6), an increase of electronic charge can be observed on the side of the Ar atom in a region that is close to the O nucleus. This suggests that the Ar atom is always pulled in the direction of the O atom, that is, toward the global minimum geometry **7** of the oxazole−Ar van der Waals complex.

We conclude that the position of the Ar atom above the ring is determined by reduced exchange repulsion at the side of the oxygen atom. Although oxygen possesses more electrons than any other atom in the oxazole ring, its negative charge is much more contracted than that of either N or C and, as a consequence, its volume is smaller.

This is confirmed by analyzing the MP2 Laplace concentration $-\nabla^2\varrho(\mathbf{r})$[45] of oxazole in the ring plane and in parallel planes shifted by 0.35, 0.5, 0.85, and 1 Å in the direction perpendicular to the ring plane (Figure 9 and Table 11).

Although the electron density is much larger above the O atom than above any other ring atom, it decreases rapidly with increasing distance to the nucleus. This becomes even more obvious when comparing the corresponding Laplace concentrations in Table 11. At all distances investigated, the Laplace concentration above the O nucleus is significantly smaller than that above any other nucleus of the oxazole ring. The contour line diagrams of the Laplace concentration taken in the ring plane (Figure 9a) and at 0.35 Å above the ring plane (Figure 9b) reveal that the regions around and above the ring center are depleted of negative charge (solid contour lines, Figure 9). These regions extend toward the oxygen atom and surround it already in the 0.35 Å plane. Hence, exchange repulsion effects are smaller in the direction of the Ar atom. The Ar atom can approach the O atom much closer than any other ring atom from above. There is a distinct hole in the π-distribution above the O atom that can be quantified by comparing the Laplace concentration values of Table 11.

The analysis of the Laplace concentration provides a basis to predict positions around a molecule at which exchange repulsion should be significantly reduced. In the case of Ar van der Waals complexes, this position determines the most stable configuration of the van der Waals complex, which can be confirmed by analysis of the difference electron density distribution as done in this work. Since exchange repulsion is in any case destabilizing, the complex has to be considered predominantly dispersion bound, although exchange repulsion effects determine the position of the Ar atom.

From these considerations it becomes clear why any position of the Ar atom in the oxazole plane leads to a less stable van der Waals complex, although such an approach would lead to stronger stabilizing inductive effects. In the plane, exchange repulsion, in particular, opposite to the in-plane lone pair electrons of O and N is rather strong. In addition, the Ar atom feels the stabilizing dispersion interactions of just three atoms, while above the ring dispersion interactions with five heavy atoms are possible.

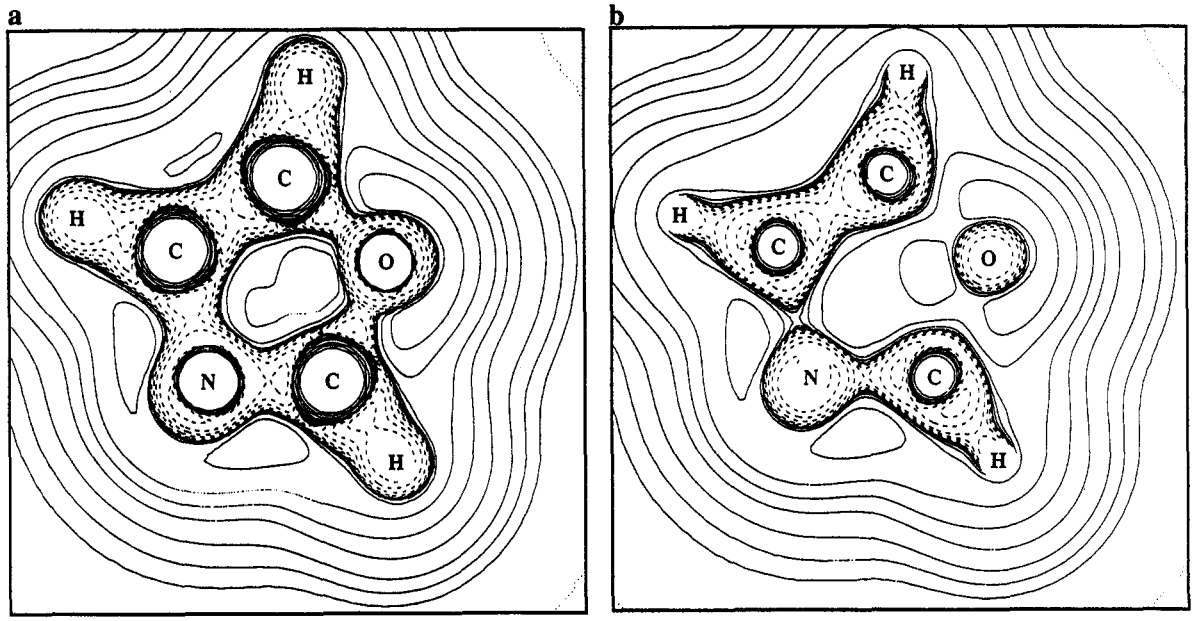

Figure 9. Contour line diagram of the Laplace concentration of oxazole, $-\nabla^2\rho(\mathbf{r})$, obtained at the MP2/6-31G(+sd,+sp) level of theory. (a) The reference plane is the plane of the ring. (b) The reference plane is the plane shifted by 0.35 Å with regard to the ring plane. Inner shell regions of the atoms are not shown. Dashed contour lines correspond to concentration of electron density, and solid lines to a depletion of electron density.

TABLE 11: MP2/6-31G(+sd,+sp) Electron Densities $\rho(\mathbf{r})$ (e/bohr^3) and Laplace Concentrations $-\nabla^2\rho(\mathbf{r})$ (e/bohr^5) at Fixed Distances above the Ring Atoms of Oxazole

	0.35 Å above ring plane		0.5 Å above ring plane		0.85 Å above ring plane		1.0 Å above ring plane		1.2 Å above ring plane	
atom	$\rho(\mathbf{r})$	$-\nabla^2\rho(\mathbf{r})$	$\rho(\mathbf{r})$	$-\nabla^2\rho(\mathbf{r})$	$\rho(\mathbf{r})$	$-\nabla^2\rho(\mathbf{r})$	$\rho(\mathbf{r})$	$-\nabla^2\rho(\mathbf{r})$	$\rho(\mathbf{r})$	$-\nabla^2\rho(\mathbf{r})$
N1	3.172	28.447	2.031	−10.208	0.504	4.600	0.265	3.232	0.097	1.126
C2	2.039	119.206	1.339	−8.118	0.444	1.859	0.255	1.739	0.096	1.040
O3	5.646	−105.032	3.042	−3.000	0.553	7.950	0.266	4.237	0.090	1.036
C4	2.057	118.620	1.357	−8.270	0.460	1.851	0.268	1.722	0.105	1.028
C5	2.000	123.313	1.319	−6.456	0.455	1.852	0.269	1.669	0.107	0.996

TABLE 12: Experimental and Calculated Dissociation Energies D (cm^{-1}) and Argon−M Distances R (Å) for a Series of Argon−M Complexes

		D [cm^{-1}]		R [Å]			
no.	complex Ar−M	exp	calc	exp	calc	shape of complex, position of Ar	references
1	Ar−H_2O	143	107	3.635	3.751	T-shaped	46 and 47
2	Ar−CO	110	108.8	3.811	3.644	T-shaped, close to C	44, 53, and 54
3	Ar−benzene	340	337	3.58	3.4−3.6	Ar above ring center	48, 49, and 50
4	Ar−fluorobenzene shifted away from F		343	3.553	3.55	Ar above ring center	51 and 37b
5	Ar−difluorobenzene	190−242	294	3.544	3.6	Ar above ring center	51 and 37b
6	Ar−pyridine			3.540		Ar above ring center shifted toward N	52
7	Ar−oxazole		304	3.485	3.580	Ar above ring center shifted toward O	this work

5. Conclusions

(1) This work has shown that, in van der Waals complexes between Ar and aromatic molecules, Ar prefers a position above (or below) the ring rather than in the ring plane, which is a result of intermolecular dispersion and exchange repulsion effects.

(2) In the oxazole−argon complex, the ring−Ar distance R_{exp} is 3.458 Å, which is somewhat smaller than the calculated MP4(SDTQ)/6-31G(+sd,+sp) and MP2/6-31G(+sd,+sp) distances R of 3.580 and 3.558 Å (at position **4**). Although experimentally it is not possible to distinguish between an Ar position closer to either the C5 or the O atom, supermolecular MP perturbation theory at 2nd, 3rd, and 4th order clearly predicts a position closer to the O atom (a = 0.226 Å, b = −0.167 Å, c = 3.538 Å) to correspond to the global minimum of the oxazole−Ar complex.

(3) The MP2 and MP4 complex stabilities are 316 and 304 cm^{-1} (904 and 870 cal/mol) at position **4**, which compares well with the calculated or measured binding energies of other Ar van der Waals complexes (see Table 12).[46−54] The oxazole−argon complex is less stable than the benzene−argon complex but comparable in stability with the difluorobenzene−argon complex. The calculated R value compares well with other R values, while the experimental R is somewhat smaller.

(4) There is no significant charge transfer between Ar and the oxazole ring, in line with our calculations in the case of benzene−Ar, Ar−CO, and fluorobenzene−Ar complexes. Contrary claims made in previous work[37] are likely due to an incorrect handling of BSSEs.

(5) The oxazole complex is predominantly stabilized by dispersion interactions while inductive effects play a minor role, which is indicated by the fact that the complex is not bound at the HF level. Besides dispersion, exchange repulsion plays an important role insofar as it determines the position of the Ar above the ring. In general, Ar moves toward the atom with the smallest volume and the smallest exchange repulsion. This is normally the most electronegative atom of a molecule with the strongest charge contraction.

(6) Our investigation shows that, besides the various energy partitioning methods, the electron density provides an excellent tool to unravel the electronic factors that determine the stability and configuration of a van der Waals complex. For example, analysis of the Laplace concentration of the monomers helps to detect regions of strong contraction of negative charge and small exchange repulsion. The difference electron density distribution of the complex, on the other hand, reveals the acting intermolecular forces by increase or decrease of electron density. In the case of complexes between Ar and aromatic molecules, one has to distinguish between situations where the density at Ar is either pulled toward the partner molecule (case I) or pushed toward the back of the Ar (case II). Oxazole−Ar belongs to case I, and benzene−Ar to case II. Distortions of the spherical Ar density distribution and that of the partner molecule explain the multipole moment components of the complex in the direction of the Ar atom.

(7) We stress that all complex properties that are investigated relative to those of the monomers have to be calculated using the CP to get reliable values. This applies not only to energy-based properties but also to any property based on the difference electron density distribution.

Acknowledgment. This work was supported by the Swedish Natural Science Research Council (NFR), the Deutsche Forschungsgemeinschaft, the Fonds der Chemie, the Land Schleswig-Holstein, and the Deutsche Akademische Austauschdienst (DAAD). All calculations were done on the CRAY YMP/464 of the Nationellt Superdatorcentrum (NSC), Linköping, Sweden. The authors thank the NSC for a generous allotment of computer time.

References and Notes

(1) For reviews see: (a) Maitland, G. C.; Rigby, M.; Smith, E. B.; Wakeham, W. A. *Intermolecular Forces*; Clarendon Press: Oxford, 1981. (b) *Structure and Dynamics of Weakly Bounded Molecular Complexes*; Weber, A., Ed.; NATO ASI Series C; Reidel: Dordrecht, 1987; Vol. 212. (c) *Dynamics of Polyatomic van der Waals Complexes*; Halberstadt, N., Janda, K. C., Eds.; NATO ASI Series B; Plenum: New York, 1990; Vol. 227. (d) Van der Waals Molecules. 1. *Chem. Rev.* **1986**, *86*, No. 6. (e) Van der Waals Molecules. 2. *Chem. Rev.* **1994**, No. 7.

(2) (a) Hirschfelder, J. O.; Curtiss, C. F.; Bird, R. B. *Molecular Theory of Gases and Liquids*; Wiley: New York, 1954. (b) Hirschfelder, J. O.; Meath, W. J. *Adv. Chem. Phys.* **1976**, *12*, 3. (c) Piecuch, P. *Molecules in Physics, Chemistry and Biology*; Kluwer Academic Publishers: Dordrecht, 1988; Vol. 2, p 417. (d) Magnasco, V.; McWeeney, R. In *Theoretical Models of Chemical Bonding (Theoretical Treatment of Large Molecules and Their Interactions)*; Maksic, Z. B., Ed.; Springer: New York, 1991; Part 4, p 133. (e) Buckingham, A. D. *Quart. Rev. (London)* **1959**, *13*, 183.

(3) Chalasinski, G.; Szczesniak, M. M. *Chem. Rev.* **1994**, *94*, 1723.

(4) Hobza, P.; Selzle, H. L.; Schlag, E. W. *Chem. Rev.* **1994**, *94*, 1767.

(5) Felker, P. M.; Maxton, P. M.; Schaeffer, M. W. *Chem. Rev.* **1994**, *94*, 1787.

(6) Jeziorski, B.; Moszynski, R.; Szalewicz, K. *Chem. Rev.* **1994**, *94*, 1887.

(7) Van der Avoird, A.; Wormer, P. E. S.; Moszynski, R. *Chem. Rev.* **1994**, *94*, 1975.

(8) Brupbacher, Th.; Bauder, A. *Chem. Phys. Lett.* **1990**, *173*, 435.

(9) Stahl, W.; Grabow, J.-U. *Z. Naturforsch. A* **1992**, *47*, 681.

(10) Kukolich, S. G. *J. Am. Chem. Soc.* **1983**, *105*, 2207.

(11) Bohn, R. K.; Hillig, K. W., II; Kluczkowski, R. L. *J. Phys. Chem.* **1989**, *93*, 3456.

(12) Gripp, J. Ph.D. Thesis, University of Kiel, 1989.

(13) MP2: Binkley, J. S.; Pople, J. A. *Int. J. Quantum Chem.* **1975**, *9*, 229. MP3: Pople, J. A.; Binkley, J. S.; Seeger, R. *Int. J. Quantum Chem. Symp.* **1976**, *10*, 1. MP4: Krishnan, R.; Pople, J. A. *Int. J. Quantum Chem.* **1978**, *14*, 91.

(14) Andresen, U.; Dreizler, H.; Grabow, J.-U.; Stahl, W. *Rev. Sci. Instrum.* **1990**, *61*, 3694.

(15) Grabow, J.-U.; Stahl, W. Z. *Naturforsch. A* **1990**, *45*, 1043.

(16) Kumar, A.; Sheridan, J.; Stiefvater, O. L. Z. *Naturforsch. A* **1978**, *33*, 145.

(17) Kumar, A.; Sheridan, J.; Stiefvater, O. L. Z. *Naturforsch. A* **1978**, *33*, 549.

(18) Van Eijck, B. P. *J. Mol. Spectrosc.* **1974**, *53*, 246.

(19) Grabow, J.-U.; Heineking, N.; Stahl, W. *J. Mol. Spectrosc.* **1992**, *152*, 168.

(20) Kraitchman, J. *Am. J. Phys.* **1953**, *21*, 17.

(21) Gordy, W.; Cook, R. L. *Microwave Molecular Spectra*, 3rd ed.; J. Wiley and Sons: New York, 1984; p 662.

(22) Spoerel, U.; Dreizler, H.; Stahl, W. *Z. Naturforsch. A* **1994**, *49*, 645.

(23) Heineking, N.; Dreizler, H.; Schwarz, R. *Z. Naturforsch. A* **1986**, *41*, 1210.

(24) Klots, T. D.; Emilsson, T.; Ruoff, R. S.; Gutowsky, H. S. *J. Phys. Chem.* **1989**, *93*, 1255.

(25) Sørensen, G. O.; Mahler, L.; Rastrup-Andersen, N. *J. Mol. Struct.* **1974**, *20*, 119.

(26) For a recent review on the basis set superposition problem, see: van Duijneveldt, F. B.; van Duijneveldt-van de Rijdt, J. G. C. M.; van Lenthe, J. H. *Chem. Rev.* **1994**, *94*, 1873.

(27) Leonard, P. J.; Barket, J. A. *Theor. Chem. (N.Y.)* **1975**, 117.

(28) Gough, K. M. *J. Chem. Phys.* **1989**, *91*, 2424.

(29) 6-31G(d): Hariharan, P. C.; Pople, J. A. *Chem. Phys. Lett.* **1972**, *66*, 217. 6-311G(d): Krishnan, R.; Frisch, M. J.; Pople, J. A. *J. Chem. Phys.* **1980**, *72*, 4244.

(30) Widmark, P. O.; Malmquist, P.; Roos, B. O. *Theor. Chim. Acta* **1990**, *77*, 291.

(31) Thakkar, A. J.; Hettema, H.; Wormer, P. E. S. *J. Chem. Phys.* **1992**, *97*, 3252.

(32) Cernusak, I.; Dierksen, G. H. F.; Sadlej, A. *J. Chem. Phys. Lett.* **1986**, *128*, 18.

(33) Raghavachari, K.; Trucks, G. W.; Pople, J. A.; Head-Gordon, M. *Chem. Phys. Lett.* **1989**, *157*, 479.

(34) Kumar, A.; Meath, W. J. *Can. J. Chem.* **1985**, *63*, 1616.

(35) Chalasinski, G.; Funk, D. J.; Simons, J.; Breckenridge, W. H. *J. Chem. Phys.* **1987**, *87*, 3569.

(36) Rosendaal, A. Internal Report, University of Utrecht, 1979.

(37) (a) Hobza, P.; Selzle, H. L.; Schlag, E. W. *J. Chem. Phys.* **1991**, *95*, 391. (b) Hobza, P.; Selzle, H. L.; Schlag, E. W. *J. Chem. Phys.* **1993**, *99*, 2809.

(38) Spackman, M. A. *J. Phys. Chem.* **1989**, *93*, 7594.

(39) Boys, F.; Bernardi, F. *Mol. Phys.* **1970**, *19*, 553.

(40) Davidson, J.; Burnham, A. K.; Siegel, B.; Flygare, W. H. *J. Am. Chem. Soc.* **1974**, *96*, 7394.

(41) Gauss, J.; Cremer, D. *Adv. Quantum Chem.* **1992**, *23*, 205.

(42) Stanton, J.; Gauss, J.; Watts, J. D.; Lauderdale, W. J.; Bartlett, R. J. Aces II, Quantum Chemistry Project; University of Florida, Gainesville, 1992.

(43) Kraka, E.; Gauss, J.; Reichel, F.; Olsson, L.; He, Z.; Cremer, D. COLOGNE94, University of Göteborg, 1994.

(44) Kukawska-Tarnawska, B.; Chalasinski, G.; Olszewski, K. *J. Chem. Phys.* **1994**, *101*, 4964.

(45) (a) Kraka, E.; Cremer, D. In *Theoretical Models of the Chemical Bond, Part 2: The Concept of the Chemical Bond*; Maksic, Z. B., Ed.; Springer-Verlag: Berlin, 1990; p 453. (b) Bader, R. F. W.; Essén, H. *J. Chem. Phys.* **1987**, *80*, 1943. (c) Bader, R. F. W.; MacDougall, P. J.; Lau, C. D. H. *J. Am. Chem. Soc.* **1984**, *106*, 1594. (d) Bader, R. F. W.; MacDougall, P. J. *J. Chem. Phys.* **1993**, *98*, 6007.

(46) Cohen, R. C.; Saykally, R. J. *J. Chem. Phys.* **1993**, *98*, 6007.

(47) Chalasinski, G.; Szczesniak, M. M.; Schreiner, S. *J. Chem. Phys.* **1991**, *94*, 2807.

(48) Krause, H.; Neusser, H. J. *J. Chem. Phys.* **1993**, *99*, 6278.

(49) Weber, Th.; Riedle, E.; Neusser, H. J.; Schlag, E. W. *Chem. Phys. Lett.* **1991**, *183*, 77.

(50) Weber, Th.; von Bergen, A.; Riedle, E.; Neusser, H. J. *J. Chem. Phys.* **1990**, *92*, 90.

(51) Su, M.-C.; O, H.-K.; Parmenter, C. S. *Chem. Phys.* **1991**, *156*, 261.

(52) Sycher, R. M.; Petitprez, D.; Bettens, F. L.; Bauder, A. *J. Phys. Chem.* **1994**, *98*, 11863.

JP950449S